Characterization of Exposures To Nanoscale Particles and Fibers During Solid Core Drilling of Hybrid Carbon Nanotube Advanced Composites

DHIMITER BELLO, BRIAN L. WARDLE, JIE ZHANG, NAMIKO YAMAMOTO, CHRISTOPHER SANTEUFEMIO, MARILYN HALLOCK, M. ABBAS VIRJI

This work investigated exposures to nanoparticles and nanofibers during solid core drilling of two types of advanced carbon nanotube (CNT)-hybrid composites: (1) reinforced plastic hybrid laminates (alumina fibers and CNT); and (2) graphite-epoxy composites (carbon fibers and CNT). Multiple real-time instruments were used to characterize the size distribution (5.6 nm to 20 μm), number and mass concentration, particle-bound polyaromatic hydrocarbons (b-PAHs), and surface area of airborne particles at the source and breathing zone. Time-integrated samples included grids for electron microscopy characterization of particle morphology and size resolved (2 nm to 20 μm) samples for the quantification of metals. Several new important findings herein include generation of airborne clusters of CNTs not seen during saw-cutting of similar composites, fewer nanofibers and respirable fibers released, similarly high exposures to nanoparticles with less dependence on the composite thickness, and ultrafine (< 5 nm) aerosol originating from thermal degradation of the composite material. *Key words*: nanoparticle, nanocomposites; fiber; CNTs; airborne exposures; occupational health; nanotechnology.

INT J OCCUP ENVIRON HEALTH 2010;16:434–450

Received from: Department of Work Environment, University of Massachusetts Lowell, Lowell, MA, USA (DB, JZ, CS); Technology Laboratory for Advanced Materials and Structures, Department of Aeronautics and Astronautics, Massachusetts Institute of Technology, Cambridge, MA, USA (BLW, NY); Environmental Health and Safety, Massachusetts Institute of Technology, Cambridge, MA, USA(MH); National Institute for Occupational Safety and Health, Division of Respiratory Disease Studies, Morgantown, WV, USA (MAV). This work was supported under the Nanoscale Science and Engineering Centers Program of the National Science Foundation (Award #NSF-0425826) and by Airbus S.A.S., Boeing, Embraer, Lockheed Martin, Saab AB, Spirit AeroSystems, Textron Inc., Composite Systems Technology, and Toho/Tenax through the Massachusetts Institute of Technology's Nano-Engineered Composite Aerospace Structures (NECST) Consortium, and under the GMMI Nanomanufacturing Program of the National Science Foundation (Award# 0800213). Namiko Yamamoto acknowledges support from the Linda and Richard (1958) Hardy Fellowship. The findings and conclusions in this report are those of the authors and do not necessarily represent the views of the National Institute for Occupational Safety and Health. Send correspondence to: Dhimiter Bello, Department of Work Environment, School of Health and Environment, University of Massachusetts, Lowell One University Ave., Lowell, MA 01854, USA; email: <Dhimiter_Bello@uml.edu>.

Disclosure: The authors declare no competing interests.

INTRODUCTION

Carbon nanotubes (CNTs) and carbon nanofibers (CNFs) offer enormous potential for development of new materials and products with superior thermal, electric, mechanical, and/or other properties. They represent a major sector of the quickly growing nanotechnology economy. The current global production of all types of CNTs and CNFs has reached hundreds of tons per year and production rates are bound to expand rapidly.[1,2] One important area of exploration of CNTs is in CNT-composites for applications in diverse sectors, such as telecommunication, energy, radiation shielding, aerospace, and defense.[3–6] Engineering of advanced hybrid composites wherein aligned CNTs are integrated into polymer matrices of existing fibrous materials is one area of fast growth in research labs around the world.

Several studies have raised serious concerns over potential toxicity of raw (unpurified) CNTs, especially those of long, straight fiber morphology. Long multi-wall CNTs have been shown to cause asbestos-like pathogenicity, such as inflammation and lesions, in mice when CNTs were introduced directly into their abdominal cavity.[7,8] Additional effects such as oxidative stress, acute inflammatory/cytokine responses, fibrosis, decrease in pulmonary function, granulomatous pneumonia, and increased susceptibility to other pollutants have been documented in mice when CNTs were instilled into their lungs or inhaled.[9–11] A range of toxicities is expected among different types of CNTs (including single-walled vs. multi-walled, raw vs. purified, long vs. short, aligned vs. tangled) and depending on production method as documented by several more recent inhalation toxicity studies.[12–15] Fiber length (particularly longer than 10 μm), aspect ratio (length/diameter ratio > 3), enhanced biopersistence in the lung fluids, as well as surface reactivity enhanced by the presence of transition metals and organics on their surfaces have been recognized as key parameters in enhancing CNT fibrogenicity and carcinogenicity.[8,16–18] The increased surface area and reactivity of nanoscale particles may also result in impaired macrophage clearance, increased bioavailability due to enhanced dissolution in biological fluids and direct access into the bloodstream, and novel pathways (such as olfactory nerve to brain shunt).

TABLE 1 Summary of Process Parameters and Measured Aerosol Properties[a]

Composite	Plies #	Thickness (mm)	Specifications Volume fraction (wt%) Al_2O_3	Epoxy	CNT	CNT (#/cm³)	Measurements and Instrumentation[b]
Base-alumina	1	1.3	44.7	55.3	–	–	• Number concentration and size distribution (fast mobility particle sizer, aerodynamic particle size, and condensation particle counter); • Mass concentration (Dust Trak); • Particle morphology and elemental composition (SEM/TEM, EDAX); • Surface area (diffusion charger); Bound PAHs (photoelectric aerosol sensor); Size selective chemical analysis for Al, Fe, Zn, Ni, Co, Cr, by ICP-MS (m2) in the breathing zone (BZ); • Respirable fibers at the source and breathing zone.
	2	2.3	67.5	32.5	–	–	
	2	2.9	44.3	55.7	–	–	
	3	2.7	61.0	39.0	–	–	
CNT-alumina	1	1.7	61.8	36.0	2.2		
	1	1.3	42.8	55.2	2.0	$\sim 2 \times 10^{12}$	
	2	2.8	53.8	44.9	1.3		
	3	3.0	52.5	45.5	2.0		
Base-carbon	22	3.9	54.5	45.5	–	–	
CNT-carbon	22	3.9	54.5	45.5	0.03	1.5×10^{11}	

[a]Diamong drill diameter: constant, 3/8"; drilling speed: 725 and 1355 RPM; drilling conditions: wet and dry.
[b]Refer to the instrumentation section in the text and Appendix B for detailed information.

The widespread uses of CNT-composites in laboratory settings for research on synthesis, uses, and testing comes with the real possibility of routine exposures to the CNTs and/or nanoparticles (NPs) generated from their processing. Yet at present only a handful of papers have directly addressed the issue of exposures to CNTs, CNFs, and NPs during synthesis and processing of new material forms containing CNTs. For example, Bello et al. found no exposures to CNTs or NPs during chemical vapor deposition (CVD) growth of the CNT forest films, their transfer out of the furnace, and their mechanical removal from the silicon support substrate.[19] In another study, low levels of micron-sized clumps of CNTs were measured during handling of the raw product (such as shovelling it out of the furnace), whereas NPs could only be generated during laboratory tests under high energy levels using a fluidized bed vortex generator.[20] Modest release of CNFs as loosely bound agglomerates has been measured during the weighing/transferring of CNFs, mechanical mixing of CNFs with the epoxy resins to form composites, and during wet-saw cutting of the polymer composites.[21] In contrast, another study indicated that dry abrasive cutting of both baseline and CNT-epoxy hybrid composites did not generate free or bundles of CNTs; however, high exposures to NPs, nanofibers, and respirable fibers were noted.[22] These few studies suggest the potential for exposure to CNTs/CNFs during various processes. More importantly, it has been shown that such exposures depend on the unique characteristics of the process itself, the material form the process is acting on, and other factors, making characterization of different processes a necessity.

Recognition of potential exposure sources to such NPs, CNTs, and respirable fibers as well as an understanding of the factors affecting exposure levels is of special importance as it will enable evidence-based and timely interventions to eliminate or reduce exposures.[23] This study focuses on identifying and quantifying exposures to CNTs and NPs associated with the processing of advanced CNT-containing composites, and evaluating the impact of process factors, including control measures, on exposure levels. An appendix of acronyms has been provided as a convenience to the reader.

METHODS

Composites

Two types of advanced CNT-hybrid composites were investigated and are summarized in Table 1 and Figure 1: (1) "fuzzy fiber" reinforced plastic laminate composite containing woven alumina fibers in each lamina with aligned CNTs grown on the surface of the alumina fibers (referred to here as CNT-alumina [CNT-A]), and (2) a graphite-epoxy prepreg system (aligned and collimated carbon fibers with an epoxy resin arranged in a layered laminate configuration) with aligned CNTs placed at the center (termed here CNT-carbon [CNT-C] composites). Samples without CNTs (baseline composites) were also investigated for comparison to the CNT hybrid composites and are referred to here as base-alumina (BA) and base-carbon (BC), respectively. The fabrication of these composites has been described previously.[24–28]

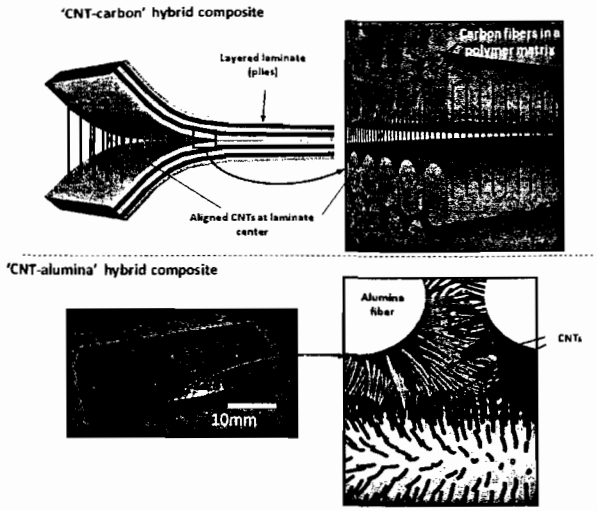

Figure 1—Illustration of the hybrid architectures used in this and prior work: (top) "nanostitched" composite with vertically aligned CNTs (VACNTs) placed in-between two plies of a laminated composite, (bottom) "fuzzy fiber" reinforced plastic (FFRP) hybrid laminate with in situ grown aligned CNTs on the woven fiber surfaces (CNTs in blue and green).

Processing of Hybrid Carbon Nanotube Composites

Laboratory setting and processes. The experimental study was conducted on a drill press (Rockwell Model 15-665) located in a laboratory with no direct air exchange with the outside environment (such as through windows or window-positioned air conditioning units).[22] The lab has instituted strict hygiene controls for all work involving processing of composites and disposal of composite wastes, including composites containing CNTs. During this entire study, the researchers wore N100 respirators and gloves. The relative humidity in the laboratory varied between 33% and 36% during the testing period.

Core drilling of composites is a common process for making holes for testing and mounting attachments, and is most typically performed using a hollow core drill, which is a hollow cylinder with diamond-grit abrasives on the circular cutting edge. Solid core drilling is used for very small diameter holes where a hollow cylinder is impractical; the solid core drill has a circular-area cutting surface. During this study we focused on four major potential exposure modifying factors: composite type (CNT-A, CNT-C, BA, and BC); drilling RPM (low, 725 rpm; and high, 1355 rpm); specimen thickness; and dry vs. wet drilling (Table 1). A constant drill rate was achieved by applying a constant force (maintained by a constant weight) on the specimen. Following preliminary testing, a 3/8" (0.95 cm) drill bit size was used for all experiments. Wet drilling was conducted on BA and CNT-A composites under conditions that had the potential to produce the highest exposures during dry drilling (that is, high drilling RPMs and thicker composites). Wetting of the composite was achieved by continuous spraying of distilled water on the composite using a spray bottle.

The processes were monitored on two different occasions over the course of one year (session one took place on April 3, 2009; session two took place on August 26, 2009). Five consecutive drills were performed on each composite sample, for each combination of experimental factors, lasting < 5 min. Ten to 30 replicate tests were available for each combination. Each experimental session lasted six hours.

Exposure characterization. A combination of real-time and integrated samples were collected at the source and breathing zone (BZ) to facilitate a comparison of the source (signature) characteristics with personal exposure characteristics. A suite of instruments was employed in order to capture several important physicochemical properties of the generated aerosol including: particle size distribution, number and mass concentration, particle-bound polycyclic aromatic hydrocarbons (b-PAHs) concentration, surface area, and microscopy analyses of integrated samples including particle size, morphology, elemental analysis, respirable fibers, and size-fractionated chemical composition to facilitate a comprehensive characterization of exposure (summarized in Appendix B).

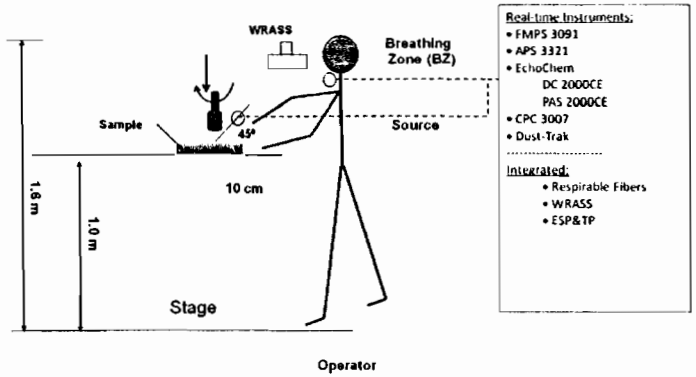

Figure 2—Schematics of the drill process and sample arrangement of personnel and equipment. For details about the instruments, please refer to the instrumentation section of this paper.

Aerosol characterization in real time. Particle size distribution and number concentration of the generated aerosols were measured using a fast mobility particle sizer ([FMPS] Model 3091, TSI Inc., St. Paul, MN) and an aerodynamic particle sizer ([APS] TSI Model 3321). These instruments cover a broad size distribution range of 5.6 nm to 20 μm and have a fast response time of one second, a critical requirement for acquiring size distributions of transient processes that last less than two minutes. A condensation particle counter ([CPC] TSI Model 3007) and a DustTrak (TSI Model 8520) were used with a one second response time to obtain measures of the total number concentration in the range of 0.01 to 1 μm, and mass concentration in the range of 0.1 to 10 μm respectively.

During the first monitoring session only, a diffusion charger ([DC] Model 2000CE, EchoChem, League City, TX) was used to measure the surface area of NPs and a photoelectric aerosol sensor ([PAS] EchoChem Model 2000CE) was used to measure b-PAHs. It has been shown that PAHs are produced during the synthesis of CNTs;[29] quantifiable amounts of several PAHs (such as fluorene, phenanthrene, pyrene, and benzo(ghi) perylene) have been measured on multiple commercial CNT samples at levels up to 30 ppm (Bello D, unpublished data).

The inlets of FMPS, APS, CPC, and DustTrak, all connected with conductive tubing (< 1 m) and bundled together, were positioned 10 cm from where the drill contacted the composite at a 45° vertical angle (Figure 2). After five replicate tests, the inlets of the instruments were switched to the BZ of the operator (~10 cm from the nose/mouth) for personal exposure monitoring and the tests were repeated again. The repositioning of instrument inlets between source and BZ was done only after airborne exposure levels had returned to background levels. Due to space constraints, the inlets of the DC and PAS instruments were positioned 5 cm behind the bundled suite of other instruments (15 cm from the source and on the same vertical plane), and remained stationary for the entirety of session one. All instruments were factory calibrated and they all passed field tests with an online high efficiency particulate air (HEPA) filter.

Integrated Sampling

Particle morphology. An electrostatic precipitator ([ESP], Spokane Laboratories, NIOSH, WA) and a thermal precipitator ([TP], Fraunhofer Institute of Toxicology, Germany) were used to collect particles directly onto transmission electron microscopy (TEM) grids for electron microscopy analysis. The TP was operated at a probe temperature of 120° C and tip temperature of 38°C. The TEM grids were 100-mesh copper with carbon film (Electron Microscopy Sciences, Hatfield, PA). The TEM grids were analyzed by TEM (Philips EM 400T and Topcon 002-B) for particle size and morphology. Elemental analysis for particles of interest was

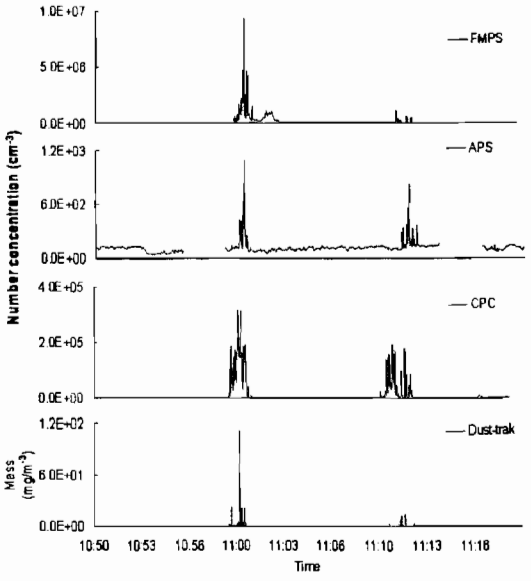

Figure 3—Illustration of the continuous monitoring instrument responses during dry drilling at 1335 RPM on three-ply 3mm thick CNT-alumina at the source (first cluster of peaks, ~11:00) and breathing zone (second cluster, ~11:12). Note the distinct responses of the condensation particle counter (CPC) and DustTrak in relation to the fast mobility particle sizer (FMPS) and aerodynamic particle sizer (APS) responses.

obtained with the integrated energy dispersive spectroscopy (EDS) detector on the Topcon TEM. An average of two TEM grids were collected for each composite type, resulting in a total of 10 TEM grids, including background samples.

Respirable fibers. Sampling for respirable fibers (length > 5 μm and aspect ratio > 3) was conducted as per NIOSH Method 7400[30] with a commercially available asbestos sampling cassette (Millipore Inc., Bedford, MA). Samples were collected both at the source and in the BZ. A wedge of each filter from the cassette was analyzed by SEM (JEOL Ltd., JSM-7401F) after gold coating and by NIOSH Method 7400 (for respirable fibers) by phase contrast microscopy. An average of two filters were collected for each composite type, resulting in a total of 10 filters including background samples.

Size selective chemical analysis. A wide-range aerosol sampling system ([WRASS], Nanenm Ltd., UK) was used to collect a single integrated area sample over the entire session for size- selective (2 nm to 20 μm on 12 stages) chemical analysis. This sampler consisted of a cascade impactor for the upper seven stages (0.25 to 20 μm) with glass slides as collection media, and a diffusion battery for the lower five stages (2 to 250 nm) with mesh net collection media.[31] Double-sided tape was used on the glass slides of the cascade impactor for easy recovery of the analytes from the glass slides and for minimizing any possible particle bounce. No evidence of particle overload was observed on any of the impactor stages. The WRASS was positioned next to the operator (25 cm away) in the BZ height (Figure 2). Two WRASS samples were collected in total, one for each session, both having an air volume of ~ 3.0 m^3 at 20 l/min.

Chemical analysis of each stage was performed for aluminum (Al), iron (Fe), and zinc (Zn), the three major metals besides silicon (Si) expected in the composites based on preliminary EDS analysis as well as analysis of the reference composite and CNTs materials. The analyses were performed with inductively coupled plasma mass spectrometry (ICP-MS) on an Agilent 7500cs ICP-MS system (Agilent Technologies, Yokogawa, Japan) based on the EPA 305IA[32] method, which uses microwave-assisted acid digestion of samples. Four reference composite materials (one for each composite type), two CNT nanoforest samples, and several media blanks were also sent to the lab for chemical analysis. In order to minimize sample losses during transport, each stage was transferred shortly after sampling into the laboratory-provided precleaned digestion vessels for ICP-MS analysis.

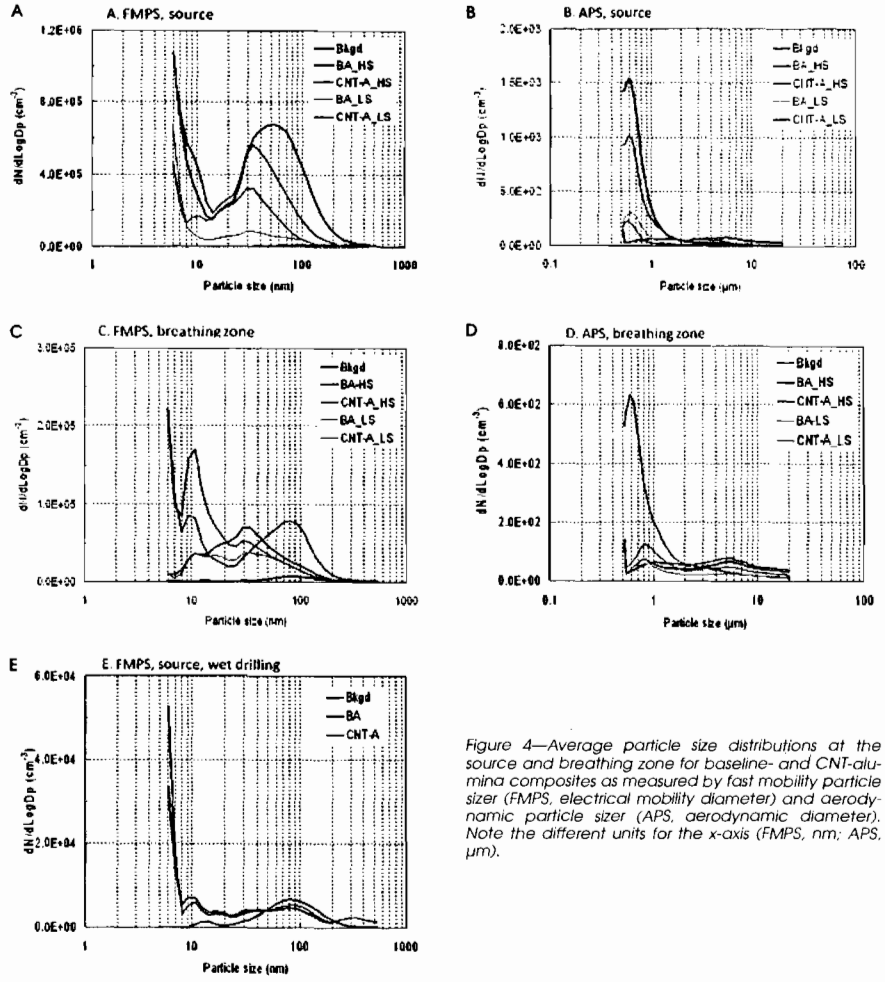

Figure 4—Average particle size distributions at the source and breathing zone for baseline- and CNT-alumina composites as measured by fast mobility particle sizer (FMPS, electrical mobility diameter) and aerodynamic particle sizer (APS, aerodynamic diameter). Note the different units for the x-axis (FMPS, nm; APS, μm).

Statistical Analysis

All data analyses were conducted in SAS v9 (SAS Inc., Carry, NC). The distributions of the mass, count, surface area, and b-PAH concentrations from the real-time instruments were examined graphically via probability plots and histograms. The data were found to be log-normal and were hence log-transformed; all analyses

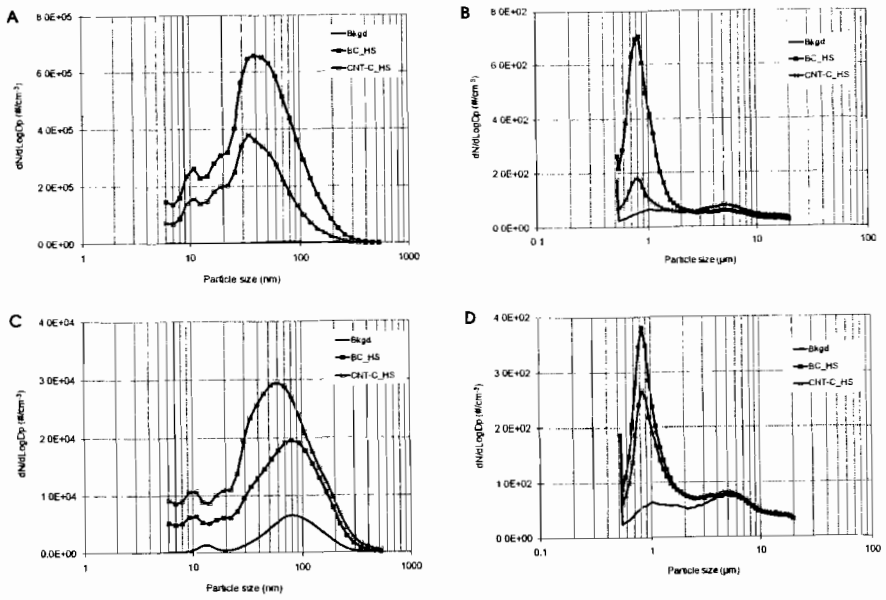

Figure 5—Average size distributions at the source and breathing zone for baseline- and CNT-carbon composites as measured by fast mobility particle sizer (FMPS, electrical mobility diameter) and aerodynamic particle sizer (APS, aerodynamic diameter). Note the different units for the x-axis (FMPS, nm; APS, μm).

were conducted on the transformed data. Real-time data from four instruments (FMPS, APS, DC, and PAS) were modeled using time-series techniques since serial measurements of short duration (1 to 10 seconds) are expected to be highly autocorrelated. The autoregressive integrated moving average (ARIMA) procedure in SAS was used to investigate autocorrelation and to test autocorrelation coefficients at different time lags, as well as to generate correlograms (plots of autocorrelation coefficients vs. time lags) and partial autocorrelation plots. The plots showed a range of exposure patterns over time in the different processes, and significant autocorrelation coefficients were observed at different time lags, but all samples consistently demonstrated a significant autocorrelation coefficient at the first time lag (first order autoregressive process). Hence summary statistics including the geometric mean (GM) and geometric standard deviation (GSD) were calculated for processes using the PROC MIXED procedure in SAS and specifying the first order autoregressive correlation structure. Lognormal particle size aerosol distributions, which are characterized by three parameters—a count median diameter (CMD), a geometric standard deviation (σ_g), and the total number concentration—were examined for each process from log-probability plots.[53]

RESULTS

Process Dynamics

Figure 3 is a typical response from multiple real-time continuous instruments and was recorded during high RPM dry drilling on CNT-A composites. The first cluster of peaks represents source emissions whereas the second cluster is the BZ concentrations for the same process. The total number concentration increased sharply as soon as the drilling tool touched the composite, but not when the tool was spinning freely, and decreased similarly when the tool retracted. The CPC response provides a good overall picture of the combined responses from FMPS and APS, an observation that was consistent throughout the study. The DustTrak lacks sensitivity to reflect changes in emissions of submicron particles and NPs during these transient processes (Figure 3).

TABLE 2 Summary Statistics of the Total Particle Number Concentration (particles/cm³) for Composites at the Source Stratified by the Process Type (Drilling Speed and Dry vs. Wet Drilling)

		Fast Mobility Particle Sizer (particles/cm³)			Aerodynamic Particle Sizer (particles/cm³)			
Composite	Process	Geometric Mean	Geometric Standard Deviation	Max	Geometric Mean	Geometric Standard Deviation	Max	Fibers (#/cm³)[a]
Background	—	4.2E+03	1.1	4.9E+03	12	1.1	137	—
Base-alumina	HS*	1.6E+05	6.8	1.0E+07	128	9.3	5602	1.3
	LS**	5.0E+04	4.5	3.6E+06	31	9.1	3877	
	HS_W***	6.8E+03	2.6	1.5E+05	16	8.0	1420	—
CNT-alumina	HS	1.8E+05	6.8	1.1E+07	96	7.4	5849	1.0
	LS	8.5E+04	4.3	3.9E+06	12	5.9	1746	
	HS_W	8.7E+03	3.4	2.0E+05	13	8.7	136	—
Base-carbon	HS	1.3E+05	7.9	4.6E+06	206	2.2	2458	1.7
CNT-carbon	HS	8.4E+04	5.1	3.9E+06	155	1.3	548	

*High speed RPM drilling (1355 rpm); **Low speed RPM drilling (725 rpm); ***Wet drilling.
[a]This includes fibers that were > 5 μm in length with an aspect ratio > 3. The data shown here are the average of two independent measurements. (m4)

Size Distribution

Alumina composites. The average size distributions for alumina composites are presented in Figure 4. Three peaks are evident, two in the FMPS and one in the APS size distributions: a (sometimes truncated) peak of < 10 nm particles, a broad peak with a maximum between 30 and 70 nm (electrical mobility diameter), and a mild third peak in APS with a maximum of 600 nm (aerodynamic diameter). The first peak, although severely truncated in the FMPS, is contributing a significant fraction to the total number concentration in FMPS. Drilling on BA at high RPMs produced the broadest size distribution at the source, with the highest normalized particle number concentration of 7×10^5 particle/cm³ at its peak size maximum of 70 nm (Figure 4A). In contrast, low RPM drilling on BA produced a 10 times smaller peak maximum, whereas CNT-A produce a peak that was twice as small. The APS size distributions were more orderly: high RPM drilling generated four to six times higher peak maxima than low RPM, whereas BA produced ~50% higher peak maxima than CNT-A (Figure 4B). The highest normalized number concentration at the peak maximum was 1500 and 1000 particles/cm³ for BA and CNT-A high RPM drilling, respectively. Based on field observations, the < 10 nm aerosol (Figures 4A, C, E) corresponded to periodically generated white smoke, which likely resulted from localized overheating and thermal degradation of the composite material. High RPM drilling on thicker composites tended to generate more smoke.

The BZ size distributions were multimodal, with at least two peak maxima in the FMPS size distributions and one in the APS (Figures 4C, D). Although they did resemble the source distributions, some differences were obvious as well. More notable was the prominence of the peaks with a maximum at ~10 nm, and the broadening, deformation, and reduced intensity of the second peak with maxima at 30–70 nm (Figure 4C). The major APS peak centered at 600 nm at the source shifted to ~800 nm for three out of four of the processes. Drilling on CNT-A at high RPMs generated the highest mean normalized number concentration of 650 particles/cm³, which was approximately five times higher than the corresponding low RPM drilling (Figure 4D). Additionally, a small peak at ~6μm was more prominent in the BZ size distributions.

Carbon fiber composites. The average size distributions for carbon composites (Figure 5, high RPM drilling only) are distinct from those of alumina composites. The most predominant peaks at the source have their maxima at 30 to 40 nm and 0.8 μm and were similar for both BC and CNT-C composites (Figures 5A, B). The BZ size distributions were similar to source distributions, except that the BZ distributions in FMPS were skewed towards larger particles (Figure 5C). Base-carbon composites produced generally higher peak maxima, both at the source and BZ. The average number concentration at the source for BC composites were 6.5×10^5 and 700 particles/cm³ in FMPS and APS, respectively. The BZ average peak maxima values for base carbon composites were 3.0×10^4 and 380 particles/cm³ in FMPS and APS, respectively. In comparison, the peak maxima for CNT-C composites were for the most part less than two times smaller than BC composites. In contrast to alumina composites, lack of particles <10 nm for carbon composites and the more orderly ranking of size distributions at the source and BZ were notable. The 0.8 μm peak for carbon composites at the source was also higher than for alumina composites.

The size distributions of the alumina and carbon composite aerosols (Figure 4A, C; Figure 5A, C) were multimodal, especially for alumina composites in the BZ, and they could not be described properly with a single lognormal distribution.

TABLE 3 Summary Statistics of the Total Particle Number Concentration (particles/cm3) at the Breathing Zone Stratified by Sampling Location and the Process Type for Each Composite

		Fast Mobility Particle Sizer (particles/cm³)			Aerodynamic Particle Sizer (particles/cm³)			
Composite	Process	Geometric Mean	Geometric Standard Deviation	Max	Geometric Mean	Geometric Standard Deviation	Max	Fibers (#/cm³)[a]
Background	—	4.2E+03	1.1	4.9E+03	12	1.1	137	—
Base-alumina	HS*	1.6E+04	4.3	7.9E+05	107	1.2	304	1.0
	LS**	1.9E+04	3.4	4.5E+05	30	10.8	433	
CNT-alumina	HS	4.6E+04	4.1	1.3E+06	59	10.4	5155	0.7
	LS	4.3E+04	6.2	2.9E+06	30	10.2	666	
Base-carbon	HS	1.0E+04	2.5	2.7E+05	195	1.5	817	1.9
CNT-carbon	HS	1.2E+04	2.9	3.8E+05	178	1.4	1100	

*High speed RPM drilling (1355 rpm); **Low speed RPM drilling (725 rpm).
[a]This includes fibers that were > 5 μm in length with an aspect ratio > 3.

Total Number Concentration

Summary statistics of the total number concentration measured by several instruments for different processes are provided in Table 2 (source) and Table 3 (BZ). The distributions of total number concentration from several tests were right skewed and could be approximated with a lognormal distribution. Each process resulted in a sharp spike in aerosol concentrations above background, both at the source and the BZ, especially for FMPS. High RPM dry drilling produced much higher total number concentrations than low RPM drilling, with GM values measured by FMPS at the source ranging from 1.6–1.8 × 10^5 particles/cm³ and GSD of seven to eight. Low RPM dry drilling produced exposures with GM in the range 5.0–8.5 × 10^4 and GSDs of ~4.5. The GM total number concentration values of FMPS for low RPM drilling at the source (available only on alumina composites) were on average 12 to 20 times higher than background, and about two to three times lower than high RPM drilling. The highest maximum FMPS total number concentration values at the source were recorded for high RPM drilling of alumina composites (~1.0 × 10^7 particles/cm³), whereas carbon composites produced a maximum value of ~4 × 10^6 particles/cm³.

The GM total number concentration (BZ) of FMPS for all processes were significantly higher than background and varied in the range 1.0–4.6 × 10^4 (GSD range 2.5 to 6.2). Alumina composites generally resulted in higher BZ exposures than carbon composites. The highest BZ total number concentration of 2.9 × 10^6 particles/cm³ was recorded for low RPM drilling of CNT-A composites, a value approximately two times higher than the second highest, high RPM drilling of CNT-A composites.

The APS total number concentration trends were slightly different than FMPS. High RPM drilling of alumina composites at the source generated higher exposures than low RPM drilling, as can be seen by the much higher (four to eight times higher) GM total number concentration values. The highest APS total number concentration maxima of > 5500 were recorded for high RPM drilling of alumina composites at the source. The APS total number concentration of carbon composites was much higher than that of alumina composites and their GSDs notably smaller (< 2.2 vs. > 6). All APS total number concentration exposures at the source were higher than background. Similar trends were seen for BZ exposures. The maximum BZ total number concentration values of 5155 and 1100 particles/cm³ were recorded for the CNT-A and CNT-C composites, respectively.

Particle Morphology

Select representative images from the TEM analysis of several grids are presented in Figure 6. Analysis by SEM of the finer dust collected from the composite surfaces at the end of drilling with double sided carbon tape (images not shown) revealed alumina and carbon fibers fractured perpendicular to the fiber axis, as well as splintered fragments along the axis, very similar to the fibers seen in Figure 6I and 6K. The finest NPs are best seen in Figures 6B and 6H, whereas the 30 to 80 nm size particles are best seen in Figure 6A, which is common in multiple TEM grids. A new finding related to the drilling of these composites, not seen with blade saw cutting, is the release of clusters of CNT aggregates, as illustrated in Figures 6E to 6G. The size of these CNT aggregates was in the respirable range (a few microns) and was found only on the TEM grids collected during drilling of CNT-composites. High aspect-ratio (fiber-like) structures with at least one nanosize dimension (Figures 6D, H) were also seen occasionally, but they were uncommon. Another interesting morphology is shown in Figure 6C, where a straight CNT bundle is attached to a much larger film fragment. The respirable fibers (> 5 μm long, aspect ratio > 3) on the filter cassette were numerous (quantitative data presented below) and were of two distinct morphologies:

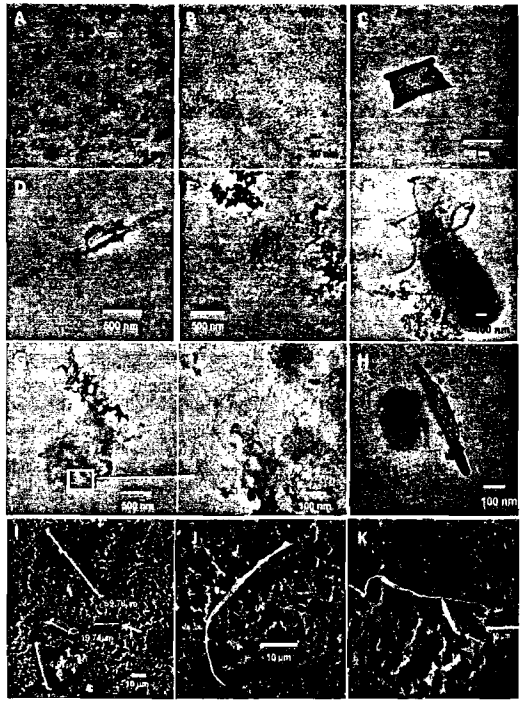

Figure 6—Select representative images of particle morphology from breathing zone samples collected during dry solid core drilling. Images 6A to 6H (TEM) originated from CNT-alumina composites. Images 6I to 6 K (SEM) originated from personal breathing zone filters collected during drilling of CNT-carbon composites and represent the most common fiber morphology for both CNT-alumina and CNT-carbon composites.

(1) straight fiber fragments of the same thickness as the parent alumina or carbon fiber (low aspect ratios) or thinner fiber splinters with a much higher aspect ratio (Figure 6I) and (2) long, thin, wavy, and rope-like structures tens of microns long (Figure 6I, J, and K). The first class of fibers (Figure 6I) was the predominant type, encompassing (based on visual observations) roughly $^3/_4$ or more of the total counted fiber number.

Respirable Fibers

Due to concerns over insufficient airborne fiber collection (thus not reaching the method limit of detection), fiber sampling was extended over high and low RPM drilling of the same composite type. Each filter collected fibers from more than two tests of five drillings for each speed (ten tests overall). Thus, sampling for BA at the source and at the BZ included a total of 40 events (eight tests × five replicates) over 45 minutes. For CNT-A, sampling included 75 events (15 tests × five replicates) over 65 minutes. The airborne concentrations of respirable fibers at the source and BZ are presented in Tables 2 and 3, respectively. The fiber concentration at the source was in the order of one fiber/cm³; BA produced a slightly higher airborne fiber concentration than CNT-A (1.3 vs. 1.0). Drilling of carbon composites (a single sample for BC and CNT-C) resulted in 1.7 fibers/cm³, indicative of similar amounts of fiber generation as with alumina composites. The BZ fiber concentrations were slightly lower than source concentrations for alumina composites and comparable for carbon composites. Because the sampling volume and the fiber surface density on the filters were below the optimal specification range of

TABLE 4 Surface Area and Particle-Bound Polyaromatic Hydrocarbons of the Nanoscale Fraction for Alumina Composites at the Source, Measured by Diffusion Charger and Photoelectric Aerosol Sensor, Respectively

		Surface Area ($\mu m^2/cm^3$)			PAHs (ng/m^3)		
	Process	Geometric Mean	Geometric Standard Deviation	Max	Geometric Mean	Geometric Standard Deviation	Max
Background		9	1.3	20	6	1.7	19
Base-alumina	HS*	25	4.4	666	8	2.4	69
	LS**	13	1.8	86	7	1.9	56
CNT-alumina	HS	51	5.7	686	10	2.4	53
	LS	23	2.9	425	6	1.9	37

*High speed RPM drilling (1355 rpm); **Low speed RPM drilling (725 rpm).

NIOSH method 7400, these fiber concentrations values should be considered as a first order approximation.

Surface Area of the Nanofraction

The DC-measured surface area (SA) varied from a background GM (GSD) of 9 (1.3) to 51 (5.7) $\mu m^2/cm^3$ for the high RPM drilling of CNT-A composites (Table 4). Consistent with previous observations from FMPS outputs, low RPM drilling produced lower SA values for both the BA and CNT-A composites. The maximum SA values of 666 and 686 $\mu m^2/cm^3$ were recorded for high RPM drilling of CNT-A and BA, respectively.

Particle-Bound Polycaromatic Hydrocarbons

The b-PAH levels for the alumina composites at the source are also summarized in Table 4. The b-PAH concentrations were moderately above background values. For example, the GM values of all processes were six to 10 ng/m^3, up to 1.7 times higher than background (GM, 6 ng/m^3) and the range of GSDs was 1.9 to 2.4. The maximum b-PAH values of 37 to 69 ng/m^3 were two to three-and-a-half times that of background (maximum value = 19). The higher values corresponded to higher peak exposures.

Size-Resolved Chemical Composition

The ICP-MS analysis of the WRASS stages for Al, Fe, and Zn for both sessions, as well as of the reference composites, is summarized in Table 5. The first visit included drilling only on alumina based composites, whereas the second visit included both alumina and carbon composites. Base alumina composites contained 25.5% Al, 0.02% Fe, and 0.47% Zn, whereas CNT-A contained 16.5 % Al, 0.21% Fe and 7.4% Zn. In contrast, the carbon composites contained much less Al, Fe, and Zn than alumina composites: each 0.005% or less. Several other metals were also analyzed (nickel [Ni], chromium [Cr], cobalt [Co], manganese [Mn], and vanadium [V]) but they were either non-detectable or were present only in trace quantities. The two major metals found in the CVD-grown nanoforests used in CNT-C composites were Fe (0.05%) and Zn (0.03%).

The majority of Al and Fe mass was found on the stages corresponding to 0.25 to 4 µm aerodynamic diameter; the metal-specific distributions for both sessions were similar. In these stages, Al varied in the range of 0.7 to 4.7 µg, whereas Fe ranged from 0.2 to 3.6 µg. Small amounts of Al and Fe were generally found in the lower stages (< 250 nm) during both sessions, except in the second session when higher amounts (1.1 µg Al; 0.5 µg Fe) were found in the < 2nm stage. Amounts of Al and Fe in the upper stages were slightly higher during the first session, a finding that is consistent with the larger number of tests conducted on alumina composites at that time and the much higher content of Al and Fe in the composites. No quantifiable Zn was found in the upper stages of the cascade impactor (amounts were marginally above blank values) during either session. However, higher amounts of Zn were found in the two to 250 nm range during the second session, ranging from 3.4 to 7.9 µg/stage. The highest amounts corresponded to the two to 60 nm range. Normalized mass distributions for each metal are plotted in Figure 7 for both sessions, in which similarities and differences are better visualized.

Wet Drilling

Wet drilling was efficient at suppressing the release of particles > 10nm (Figure 4E). However, particles < 10 nm continued to escape at high concentrations, 5.0×10^4 cm^3. This finding is consistent with the observation of smoke generation, likely resulting from the localized heating and decomposition of the internal microstructure of the hydrophobic composite.

DISCUSSION

Potential Exposures During Drilling of Advanced Composites

In this study we investigated the generation of nanoscale and submicron particles during dry and wet solid core drilling of advanced CNT-A and CNT-C fiber composites and their CNT-free counterparts. A suite of instruments was employed for real-time characterization of size distribution (5.6nm to 20µm) and total number concentration, surface area of the nanoscale fraction, particle morphology, airborne fiber concentration, and aerosol chemistry near the source and in the BZ of the operator. We investigated several potential exposure modifiers, including four composite types, two drilling RPMs, and the effect of wet drilling as a control measure. Although the study was conducted in a research laboratory, this investigation produced several important findings translatable to similar processes in a non-laboratory setting.

High exposures compared to background were measured during dry abrasive drilling of all composites (with controls off). Thus, the GM total number concentration (by FMPS) were greater than 14 (source) and 2.4 (BZ) times higher than background for all composites (not considering the wet processes). In addition to the nanoscale particles, elevated exposures were also measured in the submicron range (peak maxima, 600 to 800 nm) for all composites.

Exposure Modifiers (Determinants)

Higher input energies (such as the higher drilling RPMs, larger drill bits, and longer drill times associated with thicker composites) generally produced higher exposures. For example, the GM total number concentration values for FMPS at the source for high RPMs were about two to 3.2 times higher than for the lower RPMs. In a limited set of tests with the $^1/_4$" drill bit on BA and CNT-A, the larger drill bit ($^3/_8$") produced higher exposures (results not presented). We also noticed that drilling on thicker composites was more likely to generate a white plume of smoke (< 10 nm) as seen in real time in FMPS size distributions. This was in addition to a general increase in the number concentration of other size fractions. Therefore, one can envision that larger scale industrial operations that may use higher energy and larger composite volumes can potentially generate higher exposures than those measured in this study.

The type of composite was expected to be an important exposure modifying factor. The long aligned CNTs in the nanoengineered composites reinforced the bulk mechanical properties, and provided greater cohesion during machining (cutting or drilling). Carbon nanotube-composites generally tended to produce less exposures than their baseline counterparts, which was more prominent in the APS data (Table 2), although the differences are likely masked by other confounders such as composite thickness. Carbon-based composites produced distinct exposure distributions in the nanoscale range (FMPS) compared to the alumina composites. However, the distributions within the same composite type were similar. Additionally, the airborne respirable fiber concentrations were also similar between different composite types.

TABLE 5 Size-Resolved Metal Composition of the Aerosol Collected at the Breathing Zone with the WRASS Instrument (µg metal/stage)

			Session 1 (April 2009)			Session 2 (August 2009)		
Stage	Size Range (µm)	Media	Al	Fe	Zn	Al	Fe	Zn
1	35–20	1 × GS	7.75	1.25	< 0.06	7.05	1.55	0.48
2	20–8.1	1 × GS	1.05	1.15	< 0.04	1.45	0.05	<0.01
3	8.1–4.0	1 × GS	4.65	3.55	0.19	3.65	0.85	0.11
4	4.0–2.0	1 × GS	2.65	0.35	< 0.04	3.65	1.45	<0.01
5	2.0–1.0	1 × GS	3.85	1.25	< 0.05	1.45	0.05	<0.01
6	1.0–0.5	1 × GS	3.45	1.65	< 0.09	0.65	0.05	<0.01
7	0.5–0.25	1 × GS	1.55	1.05	< 0.04	2.55	0.15	<0.01
8	0.250–0.060	1 × PTF	0.1	0.1	< 0.01	0.3	0.5	0.75
9	0.060–0.015	10 × NYL	—[a]	—[a]	—[a]	<0.1	<0.01	7.89
10	0.015–0.005	4 × NYL	0.3	< 0.4	0.57	0.1	<0.01	6.72
11	0.005–0.002	2 × NYL	< 0.06	< 0.1	0.33	0.36	0.2	6.05
12	<0.002	1 × NYL	< 0.06	0.2	0.23	1.1	0.5	3.37
Σ			25.3	10.6	1.32	22.2	5.4	25.4
Reference Material[b] Percentage			**Al**	**Fe**	**Zn**			
Base-alumina			25.6	0.022	0.47			
CNT-alumina			16.5	0.21	7.6			
Base-carbon			0.005	0.005	7E-4			
CNT-carbon			0.001	0.003	2E-4			
CNT-nanoforest			—	0.05	0.03			

[a]Vessel ruptured during sample prep and the sample was lost. A value of < 0.1 was used for the size distribution data.
[b]The reference material was a CNT-nanoforest grown by chemical vapor deposition on a silicon substrate. Its metal composition should be the similar to the nanoforest grown on alumina composites because the process parameters are similar.

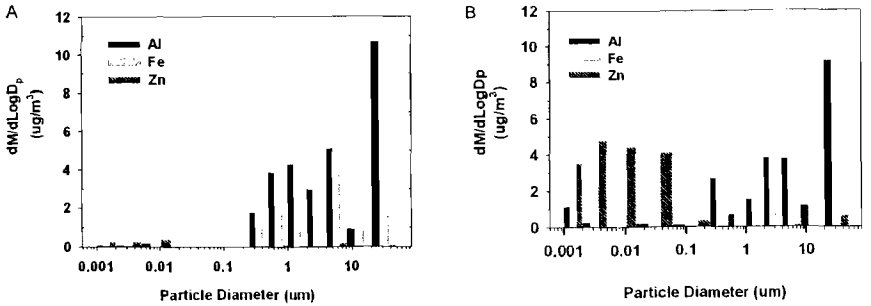

Figure 7.—Airborne mass distribution (μg/m³) for aluminum (Al), iron (Fe), and zinc (Zn), the three major metals in the alumina composites. (A) Session one: April 2009, drilling on alumina composites only; (B) Session two: August 2009, drilling on the four composite types.

Chemical Composition of the Aerosol

The sharp increase in the PAS response corresponded to the processing of composites and was high for CNT-composites at high RPM drilling. This finding suggested the possible presence of b-PAHs or other organics, consistent with the expectation that CNTs contain several PAH congeners. However, high response for the b-PAHs was also seen with BA composites. Further investigations are needed in order to draw any conclusions. It is possible that complex organic molecules may be created following high pressure and temperature curing of the epoxy polymer, as well as from thermal degradation of its components during drilling. It would be prudent to conduct targeted chemical analysis for PAHs (several of which are human carcinogens) during drilling and cutting of advanced hybrid composites, as well as during handling of CNTs. One reasonable interpretation of the b-PAHs results is that these nanoaerosols are likely to be chemically complex.

We measured acid-dissolved metals (Al, Fe and Zn in particular) as markers of different phases of the composites. The ratio of Fe in CNT-A to BA composite was 0.9, whereas that of Al was 0.35. For an equal number of tests on both composites (and assuming similar digestion efficiencies for the composite material and the NPs), one could reasonably argue that the vast majority (up to 90%) of Fe in the WRASS stages during the first session may have come from the CNT-composite. Similarly, it could be argued based on Fe content in different composites (Table 5) that CNT-A composites have likely contributed the larger portion of the airborne Fe and Zn compared to CNT-C composites. Since alumina composites contained 44% to 68% weight alumina (Table 1), the total composite mass corresponding to the measured Al would be seven to nine times higher.

Signature metals, however, provide only a limited picture of the chemical composition of the composite-derived aerosols since it is possible that a large component of the nanoscale aerosol may be originating from the degradation of the epoxy phase of the composite. Additionally, it is likely that metal exposures may be underestimated due to incomplete dissolution of the composites under the ICP-MS protocols. Dissolution is particularly more problematic for carbon-based composites. The high amounts of Zn in the nanofraction (two to 60 nm), especially during the second session, is interesting. High BZ exposures were measured on several occasions, with peak maxima in FMPS as high as some source measurements. The presence of measurable amounts of Zn and Fe in the BZ should be no surprise. However, its origin is less clear. Since Zn is more easily dissolved than Al and Fe, and the highest amounts of Zn were measured in the CNT-A composites. Zinc was the second highest in percentage of the metals in the CNTs grown in the lab, and its origin was thought to be in the impurities in the Fe salt catalysts. It is possible that a large fraction of this Zn may have originated from the CNTs themselves, although this hypothesis requires additional testing.

Energy dispersive x-ray analysis of the larger particles and thick fibers from the personal filters in SEM (SEM-EDAX, Figure 6I) matched well the elemental analysis of the bulk composite in that Al and Si (alumina composites) and C (carbon composites) were prominent in the spectra. The EDAX analysis of NPs on TEM grids (TEM-EDAX) for the most part was dominated by C with occasional pure iron oxide flakes on grids from CNT-A composites (spectra not shown), presumably originating from dipping the alumina cloth in iron catalyst salts. The EDAX of thin fibers in Figure 6J and 6K was also dominated by C, as were many other NPs. The limited sensitivity of the EDAX technique or the fact that the number of particles characterized was not representative of the billions of airborne particles may explain in part the absence of some metals (such as Zn). It is likely that a large fraction of the nanoaerosol may have originated from the organic epoxy fraction of the composite.

Drilling vs. Cutting

In a previous study, we investigated the emission of NPs during dry blade saw and wet rotary wheel cutting of the same composites.[24] Because at present there is only limited understanding regarding the influence of processes and tasks on NP exposure characteristics, a comparison between these processes is of special interest from an occupational hygiene standpoint. Although some similarities existed between cutting and drilling, differences were more prominent. Similarities worth noting included: the transitional nature of exposures consistent with short task durations, high peak exposure levels with maxima in the nanoscale and submicron fractions, the generation of respirable fibers and nanofibers, and wet processes being efficient at suppressing exposures. However, the similarities end there.

Major differences were noted in the size distributions, fiber concentration, particle morphology, observation of CNT aggregates, and the degree to which exposures were dependent on the composite types. Overall, dry abrasive drilling generated higher peak exposures than cutting (3.9×10^6 to 1×10^7 vs. 2×10^4 to 6×10^6 particles/cm³) during operations on the same composites.[21] Size distributions were also quite different. Cutting on all composite types generated similar distributions with the two sharp peaks centered at 10 to 20 nm and one μm and was quite similar for the source and BZ. In contrast, drilling generated multimodal aerosols with peaks at < 10 nm, a much broader peak at 20 to 80 nm, and a peak with a maximum at 0.6 to 0.8 μm. Distributions were strongly influenced by the composite type and were distinct for carbon and alumina composites. Profound differences were seen in particle morphology, with cutting generating far more complex particle morphologies. Most notable was the much higher frequency of nanofibers, the higher concentration of respirable fibers, and lack of CNTs (free, bundles, or ropes) generated during cutting.[22] Drilling generated fewer respirable fibers, but aggregates of CNTs were observed. Exposure distributions for drilling were severely right skewed (GSD > 5) compared to cutting (GSD < 3). Drilling generated smoke, whereas cutting did not, which was clearly illustrated in the differences in size distributions. Lastly, the composite thickness was an important modifying factor of aerosol generation intensity (total number concentration) during cutting, consistent with the volume of cutting. For drilling, thickness was less important. These differences were consistent with the processes. A simple change in the process from cutting to drilling had profound effects on the nature of nanoparticle emissions. These findings reinforce the need for systematic documentation of the nature and extent of exposures to NPs in different steps of the lifecycle of these materials because the results of one exposure scenario may not be readily transferred to another one.

Study Limitations

Several instruments were utilized in characterizing exposures to nanoscale and respirable particles generated from drilling of CNT and baseline (CNT-free) composites. The FMPS and APS cover a broad range of particle sizes, and the fast response time (one second) was an essential feature for characterizing transient aerosols associated with short-duration tasks. However, several challenges arise from three sets of issues: (1) different measuring principles utilized by these two instruments; (2) there is little overlap between their size distributions; and (3) measured aerosols are dynamic and polydisperse, with a complex particle morphology. The overlapping range (500 to 560 nm) between the two instruments is minimal, and the collection efficiency in the overlap region is poor for both instruments, making it difficult to merge the two distributions. Additionally, the FMPS measures electrical mobility diameter, whereas APS measures aerodynamic diameter. For particles of a density of ~2.2 g/cm³ (composite density), the aerodynamic diameter is ~1.4 times the mobility diameter. Hence, the measured size distributions in FMPS are likely skewed to the left, and the true aerodynamic diameters of FMPS-measured aerosols should be higher. Consistent with this prediction, recent comparisons between FMPS and several SMPSs found the FMPS to underestimate the size in the sub-100 nm range compared to SMPS. For example, 100 nm polystyrene particles were binned as 80 nm particles in FMPS.[34] In this same study, the FMPS distributions for sodium chloride aerosols were broader, whereas that of diesel exhaust were narrower than those of SMPSs. Slight variations were seen in the total number concentration and count median diameter of these aerosols as well. Lastly, uncertainties arise regarding the complex morphologies of aerosols generated during cutting and drilling of composites. For example, it is unclear in which size bins of FMPS the nanofibers and low density CNT aggregates end up. Since peak exposures were higher than the optimum range of 1×10^6 total particles/cm³ for FMPS and 1×10^3 particles/cm³ at 0.5 μm for APS, underestimation of the maximum exposures is likely. Additionally, a substantial amount of data, especially comparing the performance of various instruments, awaits further analysis.

Although we employed several techniques, including TEM/SEM/EDAX, to elucidate the chemical composi-

tion of the generated aerosol, including TEM/SEM/EDAX, b-PAHs, and conducted size-resolved analysis for several signature metals (including Al, Fe, Zn) further work is needed to better understand the contribution of each composite phase—fiber, epoxy, and CNTs—on the generation of airborne nanoaerosols and respirable fibers. Regardless, adequate exposure controls should be instituted in order to minimize long-term exposures to such aerosols both in laboratory settings and in larger-scale manufacturing operations involving composite processing.

CONCLUSIONS

Drilling on BA, CNT-A, BC, and CNT-C composites can generate significant exposures to nanoscale and submicron particles, as well as to respirable fibers. Compared to dry abrasive cutting on the same composites, drilling resulted in profound alterations of the airborne aerosol's characteristics, including size distributions, particle morphology, fiber concentrations, smoke generation, release of CNT aggregates, and lowered dependence of exposure intensity on the composite type. These findings emphasize the need for direct measurements of nanoaerosols for different processes since the prediction of exposures are difficult to make at the current level of understanding. Effective exposure controls are recommended for cutting and drilling of advanced composites containing CNTs.

The authors would like to thank Dr. Russell Dills of UW for his painstaking efforts to develop workable procedures for digestion of reference composite specimens and ICP-MS analysis, Dr. Earl Ada of the UML CMCL for his kind assistance with electron microscopy analysis needs, Dr. Arthur Miller for proving us with the prototype ESP, Drs. Aleksandr Stefaniak and Vladimir Murashov of NIOSH, and the anonymous reviewers for their constructive comments during the review of the manuscript.

References

1. Thayer AM. Carbon nanotubes by the metric ton. Chem and Eng News. 2007; 85:29-35.
2. Rakov EG. The current status of carbon nanotube and nanofiber production. Nanotechnol in Russia. 2008; 3:575-580.
3. Samal SS, Bal S. Carbon nanotube reinforced ceramic polymer composites—A review. J of Minerals and Mater Characterization and Eng. 2008, 7(4):355-370.
4. Samal SS, Bal S. Carbon nanotube reinforced polymer composites—A state of the art. Bull of Mater Sci. 2007; 30(4):379-386.
5. Khare R, Bose S. Carbon nanotube based composites—A review. J of Minerals and Mater Characterization and Eng. 2005; 4(1): 31-46.
6. Moniruzzaman M, Winey KI. Polymer nanocomposites containing carbon nanotubes. Macromolecules. 2006; 39(16):5194-5205.
7. Takagi A, Hirose A, Nishimura T, Fukumori N, Ogata A, Ohashi N, Kitajima S, Kanno J. Induction of mesothelioma in p53+/- mouse by intraperitoneal application of multi-wall carbon nanotube. Toxicol Sci. 2008; 33(1):105-116
8. Poland CA, Duffin R, Kinloch I, Maynard A, Wallace WAH, Seaton A, Stone V, Brown S, William MacNee W, Donaldson K. Carbon nanotubes introduced into the abdominal cavity of mice show asbestos-like pathogenicity in a pilot study. Nat Nanotechnol. 2008, 3(7):423-428.
9. Shvedova AA, Kisin ER, Mercer R, Murray AR, Johnson VJ, Potapovich AI, Tyurina YY, Gorelik O, Arepalli S, Schwegler-Berry D, et al. Unusual inflammatory and fibrogenic pulmonary responses to single-walled carbon nanotubes in mice. Am J Physiol Lung Cell Mol Physiol. 2005; 289(5):L698-708.
10. Li Z, Hulderman T, Salmen R, Chapman R, Leonard SS, Young SH, Shvedova A, Luster MI, Simeonova PP. Cardiovascular effects of pulmonary exposure to single-wall carbon nanotubes. Environ Health Perspect 2007; 115(3):377-382.
11. Shvedova AA, Kisin E, Murray AR, Johnson VJ, Gorelik O, Arepalli S, Hubbs AF, Mercer RR, Keohavong P, Sussman N, et al. Inhalation vs. aspiration of single-walled carbon nanotubes in C57BL/6 mice: Inflammation, fibrosis, oxidative stress, and mutagenesis. Am J Physiol Lung Cell Mol Physiol. 2008; 295(4): L552-565.
12. Ellinger-Ziegelbauer H, Pauluhn J: Pulmonary toxicity of multi-walled carbon nanotubes (Baytubes) relative to alpha-quartz following a single 6h inhalation exposure of rats and a 3 months post-exposure period. Toxicol. 2009; 266(1-3):16-29.
13. Pauluhn J. Subchronic 13-week inhalation exposure of rats to multiwalled carbon nanotubes. Toxic effects are determined by density of agglomerate structures, not fibrillar structures. Toxicol Sci. 2009; 113(1):226-242.
14. Ma-Hock L, Treumann S, Strauss V, Brill S, Luizi F, Mertler M, Wiench K, Gamer AO, van Ravenzwaay B, Landsiedel R. Inhalation toxicity of multiwall carbon nanotubes in rats exposed for 3 months. Toxicol Sci. 2009; 112(2):468-481.
15. Li JG, Li QN, Xu JY, Cai XQ, Liu RL, Li YJ, Ma JF, Li WX. The pulmonary toxicity of multi-wall carbon nanotubes in mice 30 and 60 days after inhalation exposure. J Nanosci Nanotechnol. 2009; 9(2):1384-1387.
16. Donaldson K, Aitken R, Tran L, Stone V, Duffin R, Forrest G, Alexander A. Carbon nanotubes: A review of their properties in relation to pulmonary toxicology and workplace safety. Toxicol Sci. 2006; 92(1):5-22.
17. Lam CW, James JT, McCluskey R, Arepalli S, Hunter RL. A review of carbon nanotube toxicity and assessment of potential occupational and environmental health risks. Crit Rev Toxicol. 2006; 36(3):189-217.
18. Sanchez VC, Pietruska JR, Miselis NR, Hurt RH, Kane AB. Biopersistence and potential adverse health impacts of fibrous nanomaterials: What have we learned from asbestos? Wiley Interdiscip Rev Nanomed Nanobiotechnol. 2009; 1(5):511-529.
19. Bello D, Hart AJ, Ahn K, Hallock M, Yamamoto N, Garcia EJ, M J E, Wardle BL. Particle exposure levels during CVD growth and subsequent handling of vertically-aligned carbon nanotube films. Carbon. 2008; 46:974-981.
20. Maynard AD, Baron PA, Foley M, Shvedova AA, Kisin ER, Castranova V. Exposure to carbon nanotube material: Aerosol release during the handling of unrefined single-walled carbon nanotube material. J Toxicol Environ Health. A 2004; 67(1):87-107.
21. Methner MM, Birch ME, Evans DE, Ku BK, Crouch K, Hoover MD. Identification and characterization of potential sources of worker exposure to carbon nanofibers during polymer composite laboratory operations. J Occup Environ Hyg. 2007; 4(12):D125-130.
22. Bello D, Wardle BL, Yamamoto N, Guzman deVilloria R, Garcia EJ, Hart AJ, Ahn K, Ellenbecker MJ, Hallock M. Exposure to nanoscale particles and fibers during machining of hybrid advanced composites containing carbon nanotubes. J Nanoparticle Res. 2009; 11(1):231-249.
23. Seaton A, Tran L, Aitken R, Donaldson K. Nanoparticles, human health hazard and regulation. J R Soc Interface. 2009. 7 Suppl 1:S119-129.
24. Garcia EJ, Wardle BL, Hart JA, Yamamoto N. Fabrication and multifunctional properties of a hybrid laminate with aligned carbon nanotubes grown in situ. Composites Sci and Technol. 2008; 68(9):2034-2041.
25. Garcia EJ, Hart AJ, Wardle BL, Slocum AH, Shim DJ. Aligned carbon nanotube reinforcement of graphite/epoxy ply interfaces. In: Conference Proceedings, 16th International Conference on Composite Materials (ICCM), Kyoto Japan, July 8-13, 2007.
26. Yamamoto N, Garcia E, Hart AJ, Wardle BL, Slocum A. Multifunctional characterization of aligned CNT-reinforced hybrid composites. In: Conference Proceedings, 16th International Conference on Composite Materials (ICCM), Kyoto, Japan July 8–13, 2007.
27. Yamamoto N, Hart AJ, Garcia EJ, Wicks S, Duong HM, Slocum AH, Wardle BL. High-yield growth and morphology control of aligned carbon nanotubes on ceramic fibers for multifunctional enhancement of structural composites. Carbon. 2009; 47(3): 551-560.
28. Wicks SS, Guzman de Villoria R, Wardle BL. Interlaminar and intralaminar reinforcement of composite laminates with aligned carbon nanotubes. Composites Sci and Technol. 2010; 70:20-28.
29. Plata DL, Gschwend PM, Reddy CM. Industrially synthesized single-walled carbon nanotubes: Compositional data for users, environmental risk assessments, and source apportionment. Nanotechnology. 2008; 19: 185706.
30. National Institute for Occupational Safety and Health (NIOSH). Asbestos and other fibers by PCM. Method 7400. [Internet] 1994. In: NIOSH Manual of Analytical Methods. 4th ed. Eller PM, Cassinelli ME, eds. Cincinnati, OH: NIOSH. Available from: http://www.cdc.gov/niosh/docs/2003-154/pdfs/7400.pdf.
31. Gorbunov B, Priest ND, Muir RB, Jackson PR, Gnewuch H. A novel size-selective airborne particle size fractionating instrument for health risk evaluation. Ann Occup Hyg 2009; 53(3):225-237.
32. US Environmental Protection Agency. Method 3015A. Microwave assisted acid digestion of sediments, sludges, soils, and oils. [Internet] 2007. Available from: http://www.epa.gov/osw/hazard/testmethods/sw846/pdfs/3051a.pdf.
33. Hinds WC. Aerosol technology: Properties, behaviour, and measurement of airborne particles. 2nd ed. New York: Wiley; 1999.
34. Asbach C, Kaminski H, Fissan H, Monz C, Dahmann D, Mülhopt S. Comparison of four mobility particle sizers with different time resolution for stationary exposure measurements. J of Nanoparticle Res. 2009; 11(7):1593-1609.

APPENDIX A: ABBREVIATIONS

APS:	aerodynamic particle sizer
b-PAHs:	bound polycyclic aromatic hydrocarbons
BA:	base alumina fiber composite
BC:	base-carbon fiber composite
CNF:	carbon nanofibers
CNT:	carbon nanotube
CNT-A:	CNT-alumina fiber hybrid composite
CNT-C:	CNT-carbon fiber hybrid composite
CVD:	chemical vapor deposition
ESP:	electrostatic precipitator
FMPS:	fast mobility particle sizer
SA:	surface area concentration
TP:	thermophoretic precipitator
WRASS:	wide range aerosol sampling system

APPENDIX B

Summary of Instrumentation Used in This Study for Characterization of Airborne Particles

Name (Model)	Measures	Response Time (sec)	Size Range (µm) Channels	Upper Limit	Flow Rate (l/min)
REAL-TIME SAMPLERS					
Fast mobility particle sizer (FMPS) (TSI Model 3091)	Size distribution and total number concentration (electrical mobility diameter)	1.0	0.0056–0.56 32	~1.0 × 10^6 p/cm^3	Aerosol: 10 Sheath air: 40
Aerodynamic particle sizer (APS) (TSI Model 3321)	Size distribution and total number concentration (aerodynamic diameter)	1	< 0.5–20 52	1.0 × 10^4 p/cm^3	Aerosol: 1 Sheath air: 4
Condensation particle counter (CPC) (TSI Model 3007)	Total number concentration (optical diameter)	1	0.010–1 1	~1.0 × 10^6	0.7
DustTrak, PM_{10} inlet (TSI Model 8520)	Mass concentration (particle diameter < 10 µm)	1	0.10–10 1	up to 100 mg/m^3	1.7
Diffusion charger (DC) (EchoChem Model 2000CE)	Surface orea by diffusion charging			up to 1000 tAmp	1
Photoelectric aerosol sensor (PAS) (Echo-Chem Model 2000CE)	Particle-bound polycyclic aramatic hydrocarbons by selective UV photo-ionization	1–10 sec averaging interval	< 0.100 1	1000 ng/m^3	1
INTEGRATED SAMPLERS					
Thermophoretic precipitator (TP) (Fraunhofer Institute of Toxicology, Germany)	Particle collection on a TEM grid over a pre-defined time period using a thermal gradient	NA	0.001– >100 NA	—	3.3
Electrostatic precipitator (ESP) (courtesy of Dr. A. Miller, NIOSH)	Particle collection on a TEM grid over a pre-defined time period using a point-to-plane electrostatic corona discharge	NA	0.001 – >100	—	0.1
Ride-range aerosol sampling system (WRASS) (Naneum Ltd., UK)	Particle collection and sizing of aerosol over a wide size range (0.002–20 µm) in 12 stages, five of which are in the 2–250 nm range. Subsequent chemical analysis on stages enables construction of size-selective distributions of analytes of interest (aerodynamic diameter)	NA	0.002–20 µm 12 size ranges	—	20
Fiber sampling (as per NIOSH Method 7400)	Asbestos sampling cassette (Millipore Inc., Bedford, MA); 25-mm, 0.45 µm pore size mixed-cellulose ester filter, electrically conductive 50-mm extension cowl, 2 l/min	NA	—	—	2

Note: The EchoChem instruments were available only during one of the two sessions and were stationary and positioned near the source.

Characterizing Aerosolized Particulate as Part of a Nanoprocess Exposure Assessment

JOHN T. JANKOVIC, TRACY L. ZONTEK, BURTON R. OGLE, SCOTT M. HOLLENBECK

Characterizing a process aerosol in the nanoscale beyond numeric concentration can assist in hazard assessment and in separating aerosolized process material from background aerosol. Size and size distribution, chemical composition, solubility, shape, and surface area may become important categorization parameters of exclusion/inclusion for purposes of exposure control. Various particle parameters are presented using examples from a process simulation. The process aerosol was composed of insoluble carbon particles plus environmental background constituents at an average air concentration of 2.76E+5 particles/cubic centimeter (p/cm^3). Greater than 70% of the carbon particulate was blade-like in shape, 50% of which had a height dimension ≤ 100 nm. The equivalent spherical mobility diameter of 0.8% of the particulate was ≤ 100 nm in size. The carbon blades had a root-mean-square roughness of 75 nm and an average fractal dimension of 2.25. Obtaining these measures characterizes the aerosol and identifies parameters that may be important toxicologically. *Key words:* environmental health; industrial hygiene; nanomaterials; nanoprocess exposure assessment; aerosolized particulate.

INT J OCCUP ENVIRON HEALTH 2010;16:451–457

INTRODUCTION

Nanotechnology is an expanding field that manipulates materials practically on an atomic scale. The properties of materials at the nanoscale (10^{-9} meter) may be different than what has been traditionally understood.[1] Aerosol characterization, air concentration monitoring, and establishment of workplace controls are the three components of hazard control for nanoscale materials at the Center for Nanophase Materials Sciences, a nanoscale science research center supported by the US Department of Energy (Basic Energy Sciences).[2] This work addresses the air monitoring aspects of exposure assessment. Air monitoring for nanoscale materials (NMs) is challenging. Some existing methodologies work, some old ones may need to be revised, and new approaches are under development. Occupational health and safety personnel may be asked to conduct exposure assessments of processes using or forming NMs which do not have a toxicological history, occupational exposure limit, or established sampling protocols specifying the relevant measurement parameters.[3] One of the goals of air monitoring should be to gather the type, quality, and quantity of information about the aerosol to facilitate a hazard assessment using existing or developing toxicological information for either the specific NM or NM category. This characterization should be broad in cases where little toxicological data is available since what we look for and how we look limits our observations, how we interpret them, and the specificity of the conclusions we can draw.[4]

The European Commission's Scientific Committee on Emerging and Newly Identified Health Risks deems it important for risk assessment purposes to specify clearly a number of factors: chemical composition including impurities, surface chemistry, reactivity, solubility, particle size range and distribution, shape, charge, and roughness morphology among others.[3] That this core information should be collected systematically across the NM industry is self-evident. Guidance for uniformity in specifying particle size in general and carbon nanotubes specifically are available from ASTM International.[5]

Apart from using NM aerosol characterization to judge the applicability of toxicological data for the process under investigation, NM characterization can be used to differentiate it from similarly sized background particulate. This can be accomplished by specifically measuring a chemical or morphological property inherent in the NM but absent in the background aerosol.[6] Measured total aerosol concentrations can also be adjusted to represent the nanosize concentration using the nanomaterial fraction derived from a size distribution determination.

The aerosol characterization presented here can serve as a list of particle characterization parameters for consideration when initiating air monitoring of a NM process. In addition, it may form a basis for discus-

Received from: Center for Nanophase Materials Sciences, operated for the US Department of Energy by UT Battelle, LLC, Oak Ridge National Laboratory, Oak Ridge, Tennessee, US (JTJ, SMH); Western Carolina University, School of Health Sciences, Environmental Health Program, Cullowhee, NC, US (TLZ, BRO). This research was conducted at the Center for Nanophase Materials Sciences which is sponsored at Oak Ridge National Laboratory by the Division of Scientific User Facilities, US Department of Energy (DOE). This research was supported in part by Tracy L. Zontek and Burton Ogle's appointment to the US DOE Higher Education Research Experiences for faculty at Oak Ridge Institute for Science and Education. Send correspondence to: John T. Jankovic, 1086 Southwick Drive, Alcoa, TN 37701 USA; email:<jankovicjt@hotmail.com>.

Disclosures: The authors declare no competing interests.